Aerosol physicochemical properties and implications for visibility during an intense haze episode during winter in Beijing

Y. H. Wang[1,2], Z. R. Liu[1], J. K. Zhang[1], B. Hu[1], D. S. Ji[1], Y. C. Yu[1] and Y. S. Wang[1,2]

1 State Key Laboratory of Atmospheric Boundary Layer Physics and Atmospheric Chemistry (LAPC), Institute of Atmospheric Physics, Chinese Academy of Sciences, Beijing 100029, China

2 College of Atmospheric Sciences, Lanzhou University, Lanzhou, 730000, China

*Corresponding Author: Y. S. Wang

Email: wys@mail.iap.ac.cn

Abstract

The evolution of physical, chemical and optical properties of urban aerosol particles was characterized during an extreme haze episode in Beijing, PRC, from January 24 through January 31, 2013 based on in-situ measurements. The average mass concentrations of PM_1, $PM_{2.5}$ and PM_{10} were 99 ±67μg m^{-3} (average ± stdev), 188 ±128 μg m^{-3} and 265 ±157μg m^{-3}, respectively. A significant increase in $PM_{1\text{-}2.5}$ fraction was observed during the most heavily polluted period. The average scattering coefficient at 550 nm was 877 Mm^{-1} ±624 Mm^{-1}. An increasing relative amount of coarse particles can be deduced from the variations of backscattering ratios, asymmetry parameter and scattering Ångström exponent. Particle number size distributions between 14 nm-2500 nm diameter showed high number concentrations, particularly in the nucleation mode and accumulation mode. Size-resolved chemical composition of submicron aerosol from a High Resolution-ToF-Aerosol Mass Spectrometer showed that the mass concentrations of organic, sulfate, nitrate, ammonium and chlorine mainly resided on 500nm to 800nm (vacuum diameter) particles, and nitrate and ammonium contributed greatly to particle growth during the heavily polluted day (January 28).

Increasing relative humidity and stable synoptic conditions on January 28 combined with heavy pollution on 28 January, lead to enhanced water uptake by the hygroscopic submicron particles and formation of secondary aerosol, which might be the main reasons for the severity of the haze episode. Light scattering apportionment showed that organic, sulfate, ammonium nitrate and ammonium chloride compounds

contributed to light scattering fractions of 54%, 24%, 12% and 10%, respectively. This study indicated that the organic component in submicron aerosol played an important role in visibility degradation during the haze episode in Beijing.

1. Introduction

Atmospheric aerosol particles play a significant role in radiation balance and climate forcing through direct scattering and absorption of solar radiation (Anderson et al., 2003; Poschl, 2005; Ramanathan et al., 2001). In addition, they can act as cloud condensation nuclei (CCN) and thereby change the cloud albedo and lifetime (Twomey, 1977). Accordingly, the radiative properties of clouds are indirectly influenced by aerosol (Kaufman et al., 2005; Koren et al., 2005; Lohmann and Feichter, 2005). Furthermore, the general public has to pay special attention to atmospheric aerosol due to its deleterious effect on human health and degradation of visibility (Nel, 2005; Watson, 2002), which are closely related to the chemical components, morphology, mixing state, size distribution and hygroscopic properties of aerosol particles.

Along with the rapid economic growth in China, its capital city Beijing has suffered substantially from air quality deterioration and visibility degradation, though the mass concentration of PM_{10} has decreased in Beijing in the last ten years (Liu et al., 2015). Accompanied by frequent fog-haze days, the visibility in Beijing has decreased dramatically to an unacceptable level. The frequency of visibility between 2km and 10km has increased from 37% in 1999 to 43% in 2007. (Zhang et al., 2010; Zhang et al., 2012). The mass loading of fine aerosol particles and their precursors (e.g. NH_3,

volatile organic compounds (VOCs), SO_2 and NO_x), can accumulate to high levels within the planetary boundary layer , especially during periods of persistent synoptic scale stagnation and strong temperature inversions (Zhang et al., 2013). In the past decade, many research projects have been done to characterize the chemical and physical properties of aerosol particles in Beijing and its surrounding regions. These studies mainly focused on the following aspects:

i) Chemical composition, evaluation and sources apportionment based on filter sampling and Aerosol Mass Spectrometry (AMS) (Huang et al., 2010b; Sun et al., 2006; Zhang et al., 2014) .

ii) Mass concentration and optical properties of aerosol particles using in-situ measurements or combined with MODIS (Moderate Resolution Imaging Spectroradiometer) satellite remote sensing optical depth products (He et al., 2009; Huang et al., 2010a; Li et al., 2010; Qu et al., 2010; Wang et al., 2012a; Yang et al., 2009).

iii) Aerosol hygroscopic properties, number size distributions, mixing state and implications for CCN activity, visibility, new particle formation, air pollution and radiative forcing (Chen et al., 2012; Cheng et al., 2012; Deng et al., 2013; Liu et al., 2013; Ma et al., 2012; Meier et al., 2009; Pan et al., 2009; Quan et al., 2011; Wehner et al., 2008; Wu et al., 2007; Zhang et al., 2011; Zhang et al., 2010).

The above mentioned studies, based on either long-term or short-term observations provide us with comprehensive knowledge of aerosol properties on days with near

average aerosol concentration levels. However, only a few studies were carried out on highly polluted days, and these studies mainly focus on variations of chemical composition with the evaluation of synoptic conditions and planetary boundary layer dynamics. (Huang et al., 2010a; Wang et al., 2012b; Zhao et al., 2013). The interaction between chemical and physical properties of aerosols was seldom investigated during haze episodes. Therefore, comprehensive studies of physical, optical and chemical properties using high resolution measurements are necessary for a better knowledge of aerosol evolution processes and related visibility degradation during pollution episodes in Beijing.

An intense pollution episode occurred in central and eastern China from January 24 through 31, 2013. The hourly average PM_{10} exceeded 600 μg m^{-3} and non-refractory submicron particle (NR-PM_1) exceeded 400 μg m^{-3} (Wang et al., 2013), which was the most extreme haze episode in Beijing in the last decades as far as we know. In this study, we investigated the evolution of physical, chemical, and optical properties of urban aerosol particle during the haze episode by using the in-situ measurements.

2. Methodology

2.1 Site information and instrumentation

The aerosol sampling site was situated on the roof (about 15m height above the surface) of a laboratory building in the yard of the Institute of Atmospheric Physics (IAP), Chinese Academy of Sciences, which was located between the 3rd and 4th ring roads of northeast Beijing (Zhang et al., 2014).

An integrating nephelometer (Model 3563, TSI inc., Minnesota, USA) was used to measure the total light scattering and hemispheric back scattering coefficients (for angles of 7 °to 170 °and 90 °to 170 °, respectively) of low RH aerosol at wavelengths of 450, 550 and 700nm, no size-selective inlets were used. The nephelometer was operated at 5L min^{-1} with data resolution of one minute. A calibration was conducted every month with filtered air and CO_2 as prescribed by the manufacturer. Subsequently, the data were corrected for truncation errors and the non-lambertian light source based on the measured Ångström exponents (Anderson and Ogren, 1998). On average, the corrected values were within 10% of the measured values. The mass concentration of PM_{10} and $PM_{2.5}$were measured by a Thermo TEOM 1400AB/8500 FDMS (Filter Dynamic Measurement System). The mass concentration of PM_1 was determined using a Thermo TEOM 1400.

The particle number-size distribution between 14nm and 2500nm diameter was measured by a Scanning Mobility Particle Sizer (SMPS, TSI inc., Minnesota, USA), comprising of a model TSI 3080 electrostatic classifier and a model TSI 3775 condensation particle counter (CPC), and an Aerodynamic Particle Sizer (APS, Model 3321, TSI inc., Minnesota, USA). The SMPS data covered the particle size range from 14nm to 533nm, and the APS covered from 542 nm to 2500nm. The size-dependent diffusional and gravitational losses for the inlet line have been corrected by using the empirical functions given by Willeke and Baron (1993). The data collected from these two instruments were merged into one particle size spectrum matrix (14nm to 2500nm) according to the methods of Liu et al. (2014) and Beddows et al. (2010).

The aerosol chemical composition was acquired using an Aerodyne High-Resolution Time-of-Flight Aerosol Mass Spectrometer (HR-ToF-AMS, or AMS, Aerodyne Research Inc., Billerica, MA, USA). The organic matter, sulfate, nitrate, ammonium and chlorine in non-refractory submicron particle mass-size distributions (NR-PM_1) were determined under V and W ion optical modes alternatively every 7.5 minutes. Detailed information of data analysis, collection efficiency (CE) and relative ionization efficiency of the instrument were introduced by Zhang et al. (2014). Simultaneously, the gaseous pollutants (e.g., NO, NO_x, CO, O_3 and SO_2) were measured using Thermo instruments (series of 42i, 48i, 49i and 43i, respectively, Thermo Fisher Scientific, Franklin, Massachusetts, USA). Detailed introduction and calibrations were given by (Tang et al., 2012; Wang et al., 2014).

An automatic meteorological observation instrument (Milos520, Vaisala, Finland) was used to obtain meteorological parameters (relative humidity, air temperature, wind speed and direction). The time base for all data in the study was Beijing zone time (UTC+8).

3. Results and discussion

3.1 Aerosol mass concentration and meteorological parameters

Figure 1 shows the mass concentrations of PM_1, $PM_{1\text{-}2.5}$, $PM_{2.5\text{-}10}$ and mass concentration ratios of $PM_1/PM_{2.5}$, $PM_{2.5}/PM_{10}$ during the period. The average mass concentrations of PM_1, $PM_{2.5}$ and PM_{10} are $99.1 \pm 67.1 \mu g\ m^{-3}$, $188.3 \pm 128.8\ \mu g\ m^{-3}$ and $265.2 \pm 157.1 \mu g\ m^{-3}$, indicative of the high level of aerosol pollution. The average

mass ratios of $PM_1/PM_{2.5}$ and $PM_{2.5}/PM_{10}$ are 0.56 ± 0.16 and 0.64±0.15, respectively. As we can see in Figure 1(b), the mass ratio of $PM_1/PM_{2.5}$ is higher than that of $PM_{2.5}/PM_{10}$ before January 28, indicating that PM_1 dominated the total mass. The aerosol concentration increased gradually and reached the maximum values at12:00 of January 29, with PM_1, $PM_{2.5}$ and PM_{10} values of 243.1μg m^{-3}, 504.6μg m^{-3} and 620.8μg m^{-3}. The detailed interpretations of the high values will be presented in following section. Thereafter, the aerosol concentrations decreased rapidly to a lower level. The mass ratios of $PM_1/PM_{2.5}$ and $PM_{2.5}/PM_{10}$ showed opposite pattern with time variation during the period, indicating a decreasing fraction of PM_1 compared with $PM_{2.5}$ and an increasing fraction of $PM_{2.5}$ compared with PM_{10} with increasing aerosol pollution. It is worth noting that the increase of $PM_{1-2.5}$ was greatest during the period January 28 to 29, as showed in Figure 1(a). Figure S1 displays meteorological parameters during the episode. During this period, the average wind speed was 2.5 m/s. Figure S2 shows an overview of wind rose of the local wind and the wind is mainly in the southerly and northerly quadrant, which can bring relative dirty or clean air masses, respectively. Figure 2 exhibits 72 hours backward trajectories of air parcels every 3hours using Hysplit model from a height of 100m, with a total of six clusters yielded (http://ready.arl.noaa.gov/HYSPLIT.php). We should clarify that the southern area of Beijing often suffers more polluted atmosphere than that in the northern area due to more cities and population. The clusters of 1 to 5 are from the northerly direction, with clean air and high transport height. Furthermore, a long transport pathway within 72 hours implies that those air parcels have a higher

transport speed compared with cluster 6. The cluster 6, from southern and local directions with a fraction of 47%, has the highest frequency. The cluster has a short transport distance of nearly 400 km, low transport height and speed, resulting in a sufficient loading of surface air pollutions compared with other clusters. We also present sounding data in Beijing from University of Wyoming twice a day (http://weather.uwyo.edu/upperair/), as shown in Figure 3. These lines with different colors represent soundings during the observation period. It is worth noting that an inversion layer between 1000m to 1500m exists after January 27th. Particularly at 08:00 of 28th (Beijing time), the lapse rate of temperature is nearly 0.6℃/100m, which indicates a very stable synoptic condition. Combined with low wind speed shown in figure S1, the horizontal motion is also limited during the pollution episode.

3.2 Aerosol optical properties

The aerosol scattering coefficient (σ_{sp}) and backscattering coefficient (σ_{bsp}) can be directly measured by the nephelometer and then aerosol backscattering fraction (b_λ), scattering Ångström exponent ($Å_{sp}$) and asymmetry parameter (g_λ) can be calculated from the scattering coefficients, which have rarely been reported in Beijing using in-situ measurements. The aerosol light scattering coefficients show the same pattern as mass concentration of PM, as shown in Figure 4. Table 1 shows the statistics of the aerosol optical properties during this haze episode, and the average aerosol scattering coefficients σ_{sp}^{450}, σ_{sp}^{550} and σ_{sp}^{700} are 1088.5±748.1Mm^{-1}, 877.2 Mm^{-1}±624.2 Mm^{-1} and 718.4 Mm^{-1}±530.8 Mm^{-1}, respectively. After converting the aerosol light scattering coefficients at 550nm to that of 525nm, the average σ_{sp} at 525nm are 3.2

174 times greater than the yearly average values at another site in Beijing, reported by He
175 et al. (2009). The average aerosol backscattering coefficients σ_{bsp}^{450}, σ_{bsp}^{550} and σ_{bsp}^{700} are
176 134.4 Mm^{-1} ±87.1 Mm^{-1}, 108.1 Mm^{-1} ±71.1 Mm^{-1} and 98.7 Mm^{-1} ±66.5 Mm^{-1},
177 respectively, as presented in Figure 4 (b). During the whole campaign, σ_{sp} and σ_{bsp}
178 at three wavelengths were highly correlated. Both σ_{sp} and σ_{bsp} increase gradually
179 from 24 to 29 January and decrease sharply to lower levels, which are consistent with
180 the variations of aerosol mass concentrations.
181 The backscattering ratio, which is also called the hemispheric backscatter fraction, is
182 the ratio of light scattered in the backward hemisphere to the total light scattered by
183 particles. It is related to particle size distribution and can be calculated as following;

184 $$b_\lambda = \frac{\sigma_{bsp}^{\lambda}}{\sigma_{sp}^{\lambda}} \quad (1)$$

185 The average b_λ at three wavelengths are 0.13 ±0.02, 0.14 ±0.02 and 0.15 ±0.02,
186 respectively. A higher value of b_λ at 700nm indicates relatively more small size
187 particles that scatter light in the backward hemisphere. The scattering Ångström
188 exponent ($Å_{sp}$) represents the wavelength dependence of scattering coefficient and is
189 related to the slope of the number-size distribution or the mean size and relative
190 concentrations of the accumulation and coarse mode aerosol. It is calculated using any
191 two of three channels as following;

192 $$\overset{0}{A} = -\frac{\log(\sigma_{sp}^{\lambda_1}) - \log(\sigma_{sp}^{\lambda_2})}{\log(\lambda_1) - \log(\lambda_2)} \quad (2)$$

193 The average $\overset{0}{A}_{450/550}$ and $\overset{0}{A}_{550/700}$ are 1.2 ±0.3 and 0.94 ±0.3, respectively. The average
194 $\overset{0}{A}_{450/700}$ is 1.1 ±0.3, which is smaller than that of 1.46 in Guangzhou (Garland et al.,

2008) and 1.7 in Spain reported by (Titos et al., 2012), which indicates a more dominant coarse mode particle compared with the other locations.

The asymmetry parameter g is a fundamental parameter for radiative transfer calculation, and is defined as the intensity-weighted averaged cosine of the scattering angle:

$$g_\lambda = \frac{1}{2}\int_0^\pi \cos\theta P(\theta)\sin\theta d\theta \quad (3)$$

Where θ is the angle between incident light and scattering direction and P (θ) is the angular distribution of scattered light (the phase function). The value of g_λ ranges between -1 for completely backscattered light to +1 for completely forward scattered light. Because there is no measurements method that can directly obtain the values of g, a fit equation applied by Andrews et al. (2006) was used as in equation 4.

$$g_\lambda = -7.143889 * b_\lambda^3 + 7.464439 * b_\lambda^2 - 3.9356 * b_\lambda + 0.9893 \quad (4)$$

The average value of g_λ at 450nm, 550nm and 700nm are 0.58 ± 0.04, 0.59 ± 0.05 and 0.54 ± 0.05, respectively. The three parameters of b_λ, $Å_{sp}$ and g_λ can show a relative contribution of particle size to light scattering. During 24 and 25 January, b_λ and $Å_{sp}$ shows higher values, which shows lower ones, as showed in Figure 4. However, the opposite feature occurs when the haze developed. Especially during the highest pollution periods (from 28 to 30 January), higher values of b_λ, $Å_{sp}$ and lower values of g_λ appear, which indicates an increasing fraction of relative coarse aerosol, consistent with the variation pattern of $PM_1/PM_{2.5}$ showed in Figure 1(b).

3.3 particle number size distribution

The particle number-size distribution from January 25 to 31 is shown in Figure 5(a).

The particle number concentration peaks at a diameter of around 100 nm. These particles are mainly from direct emissions of vehicles, cooking and new particle formation (Shi et al., 2001). Particle volume concentration and mass concentration are shown in figure 5(b) and (c), respectively, assuming an average aerosol bulk density of 1.5 g.cm^3 and that all particles are regular spheres based on the research by (Zhang et al., 2004) in Pittsburgh PA, USA. The coarse mode particles between diameters of 1000nm to 2500nm increased significantly during the most heavily pollution periods (28 and 29 January), as shown in Figure 5 (b) and 5 (c), which is consistent with interpretations of variation ratio of $PM_1/PM_{2.5}$. The time series of calculated mass concentration of $PM_{2.5}$, number concentrations of nucleation mode (14nm-25nm), Aitken mode (25nm-100nm), accumulation mode (100nm-1000nm) and coarse mode (1000 nm-2500nm) are presented in Figure 6. The calculated mass concentration of $PM_{2.5}$matches well with measured values, with R^2 values of 0.97, as shown in Figure S3. The nucleation mode particles show the highest number concentration during the period, with an average value greater than1.5×10^6 cm^{-3}, indicating large emission of reactive or low volatility, aerosol precursor gases (e.g. sulfur dioxide and organic vapors). The lowest particle number concentration is in coarse mode (D_m>1000nm), with an average value of 3.18×10^3 cm^{-3}. The Aitken mode and accumulation mode also show high number concentrations, with the average values of 1.90×10^5 cm^{-3} and 1.01×10^6 cm^{-3}. Compared with three years of measurements of particle number concentration at another urban site in Beijing, the number concentrations of nucleation, Aitken and accumulation mode during this haze episode are more than 170

239 times, 10 times and 120 times, respectively (Hu et al., 2009). The nucleation mode
240 and Aitken mode particle show a significant increase at mid-day on 28 January, while
241 the accumulation mode is not significant. This may be ascribed to the emissions from
242 vehicle and cooking nearby our sampling site. It is worth noting that the concentration
243 of coarse mode particle was highest on the 28th and 29th of January, which is
244 consistent with the pattern of $PM_{2.5}/PM_{10}$. After the coagulation, condensation and
245 hygroscopic growth, the number concentrations of nucleation mode and Aitken mode
246 particle decrease on 12:00 of 30 January, as shown in Figure 6.

247 **3.4 aerosol chemical properties**

248 The time series of chemical compositions, mass fractions, O:C ratio and m/z 44 of
249 NR-PM_1 are presented in Figure7(a), (b) and (c). The average mass concentrations of
250 organic, sulfate, nitrate, ammonium and chloride are $62.1 \pm 46.1 \mu g\ m^{-3}$,
251 $28.4 \pm 22.1 \mu g\ m^{-3}$, $37.2 \pm 30.6 \mu g\ m^{-3}$, $17.4 \pm 12.7 \mu g\ m^{-3}$ and $5.5 \pm 4.2 \mu g\ m^{-3}$, respectively.
252 The organic component is dominant in NR- PM_1, with an average mass fraction of
253 44.9% ±11.7%. Sulfate and nitrate species concentrations are also very high during the
254 heavy haze event.

255 AMS enables the real time determination of size-resolved chemical compositions of
256 different modes of particles as a function of time. Figure 8 shows the temporal
257 variations of the size distributions of the organic (a), sulfate (b), nitrate (c),
258 ammonium (d) and chloride (e). The organic and chloride containing particles display
259 a slightly broader distribution than the other three species. All the aerosol components
260 mainly reside in the accumulation mode with vacuum aerodynamic diameters around

700nm. Note that the AMS size distributions here are shown as a function of vacuum aerodynamic diameter, D_{va}, which is the aerodynamic diameter measured under free-molecular regime flow conditions. To a first approximation, 700nm in D_{va} corresponds roughly to 470 nm in physical diameter for spherical particles. It is worth noting that particles with optical diameters between 100nm and 1000nm have the highest scattering efficiency in the visible range (Liou, 2002), so a high concentration at this optimum aerosol size will lead to strong light scattering and reduced visibility during the period.

These five aerosol components all show high concentrations from the afternoon of 28 January to noon of 29 January, corresponding with the highest mass loading and light scattering of the whole pollution period. The detailed behaviors of particle number concentration, size-resolved organic, sulfate, nitrate, ammonium and particle mass concentration on January 28 are presented in Figure S5 and S6. The particle number concentrations show a burst at nearly 12:00, with D_m less than 100nm. Observations by Sakurai et al. (2005) in Atlanta, GA, USA recognized this as a plume related to a new particle formation event, which was accompanied by advection of local emissions. However, an increasing concentration of aerosol chemical components at about 11:00 on 28 January is observed by the AMS as shown in Figure S5. The mass concentrations mainly reside on between 300nm and 1000nm in vacuum diameter. This may be due to the accumulation of air pollutants in the stagnant boundary layer. As we can see in figure S1, the meteorological parameters are characterized by calm wind, low RH and increasing temperature in the morning,

which leads to a stable boundary layer. Then, with increasing surface temperature and PBL height, the dilution causes the aerosol concentration decreasing in the afternoon. The concentrations of sulfate, ammonium and nitrate show an increasing trend from 18:00. The major reasons are: (1) Increasing RH may enhance the heterogeneous reaction of SO_2 and NH_3 to produce sulfate and nitrate. (2) Decreased PBL height at night leads to accumulation of air pollutant. (3) Conversion of N_2O_5 to nitrate via heterogonous or homogenous ways and reaction of OH and NO_2 (Kim et al., 2014). All of the above aspects result in the mass concentrations of nitrate and ammonium having a distinct growth of particles with diameters between 100nm and 500nm on 28 January.

3.5 Increased formation of Secondary Organic Aerosol (SOA) during haze pollution episode

Figure 10 shows the variations of signal of m/z 44 as a function of organic aerosol mass concentration and the influence of relative humidity. The frequency distributions of organic mass and m/z 44 during the period are presented as well. The greatest frequency of occurrence of organic aerosol concentration appears nearly between mass concentrations of 20 to 35μg m^{-3}, corresponding with signal fraction of m/z 44 less than 2. The signal of m/z 44 shows an increasing trend with increasing organic mass. The lower concentration of organic component mainly exists at RH below 40%, which is indicative of a relatively clean atmosphere in urban Beijing. It is notable that the higher levels of the organic component occur under high RH conditions, of when aerosol water

uptake ability is enhanced and the more highly hydrated particles are able to capture more water-soluble volatile organic compounds (VOCs). In this way, the dry mass concentration of organic aerosol increases after the water evaporated in the AMS. The studies of Ge et al. (2012) in central valley of California and Dall'Osto et al. (2009) in London also showed that aqueous-phase processes are responsible for the production of secondary organic aerosol species, most significantly during fog events.

3.6 Light scattering apportionment

Light scattering by atmospheric aerosols is highly dependent on their size, morphology and compositions (Liou, 2002). Sulfate, nitrate, ammonium and organic components in aerosol contribute most to light scattering, and particularly for diameters ranging from 100nm to 1000nm, they have the greatest light extinction efficiency (Seinfeld and Pandis, 1998). Here, a modified IMPROVE algorithm was employed to apportion light scattering coefficients at λ=550nm (Pitchford et al., 2007). The IMPROVE algorithm was based on a multiple liner regression method (Chan et al., 1999), which considers the degree to which aerosol light scattering is related to the mass concentration of each component combined with water uptake of inorganic component. The detailed introduction of the method can be can be found in Lowenthal et al. (1995).The f(RH) curve obtained by Chen et al. (2014) during January in Northern China Plain is used here.

In our light apportionment calculation, the mass concentrations of ammonium sulfate, ammonium bisulfate, ammonium nitrate, ammonium chloride and organic were

327 required. However, the AMS can only provide us with mass concentrations of sulfate,
328 nitrate, ammonium chloride and organic compounds. Here, a commonly accepted ion
329 pairing scheme of calculating the neutral aerosol from the molar number of all ions
330 simplified by Gysel et al. (2007) is applied. In this scheme, by setting the fraction of
331 nitric acid to zero, the molar fraction of ammonium nitrate is equal to the molar
332 fraction of nitrate ions. The rest of ammonium ions are assigned to ammonium
333 bisulfate, ammonium sulfate and ammonium chloride according to ammonium molar
334 fraction.
335 In the IMPROVE algorithm, the light scattering growth due to inorganic components
336 were considered, while the contribution from organic aerosol did not take into account.
337 Then, using the highly resolution mass concentrations of sulfate containing aerosol,
338 ammonium nitrate, ammonium chloride and organic in submicron aerosol and aerosol
339 scattering growth curve, we calculated a relationship of scattering coefficient and
340 aerosol components and light scattering growth factor as showed in formula 9 . The
341 fitting was computed with MATLAB software (MATLAB R2010a). Figure 11 (a)
342 shows the time series of apportioned light scattering coefficients of each of the
343 aerosol components compared with measured values during observation period. At the
344 beginning of the periods, organic components dominated light scattering. With the
345 development of the haze, the contribution of inorganic components increased as
346 shown in Figure 11 (b). The total average light scattering contribution of each aerosol
347 component is presented in Figure 12. The apportionment contributions from organic,
348 sulfate, ammonium nitrate and ammonium chloride were 54%, 24%, 12% and 10%,

respectively, which indicated the dominant contribution of organic and sulfate compounds to light scattering during this haze episode in Beijing. One should note that the apportioned light scattering coefficient using the IMPROVE method is highly related with its mass concentration, and organic aerosol is a large fraction of the mass. Yao et al. (2010) showed that the organic components contributed greatly to the light extinction (about 45% contribution) by using AMS data during winter in Shenzhen, PRC. Watson (2002) also found the organic aerosol dominated light extinction in some cities, with fractions of 9%～50% in east USA.

$$\sigma_{sp}^{550} = 6.5f(RH)[(NH_4)_2SO_4] + 6.5f(RH)[NH_4HSO_4] + 2.2f(RH)[NH_4NO_3] + 4.3f(RH)[NH4Cl] + 5.7[organic] + 57.3 \quad (9)$$

4. Summary and Conclusion

Based on in-situ measurements, the physical and chemical properties of aerosol particles were characterized during a severe haze episode in Beijing from 24 January to 31January during, 2013. The average mass concentrations of PM_1, $PM_{2.5}$ and PM_{10} were 99.1±67.1μg m^{-3}, 188.3±128.8 μg m^{-3} and 265.2±157.1μg m^{-3}, respectively, and an increasing fraction of $PM_{1\text{-}2.5}$ was significant during the most heavy pollution periods. The averaged scattering coefficient at 550 nm was 877.2 Mm^{-1}±624.2 Mm^{-1}, and an increasing amount of relative coarse particle also can be seen from the variations of backscattering ratios, asymmetry parameter and scattering Ångström exponent. Particle number size distribution (14 nm to 2500nm) showed high number concentrations in the nucleation and accumulation modes. Size-resolved chemical composition of submicron aerosol from a HR-ToF-AMS showed that the mass concentration of organic, sulfate, nitrate, ammonium and chlorine mainly resided on

500nm-800nm in vacuum diameter, and sulfate and ammonium contributed to the growth of particle during the most heavily polluted day on January 28.

High emissions of regional background pollutants combined with stable synoptic conditions and increasing of relative humidity, which lead to enhanced water uptake ability of submicron aerosol and formation of secondary aerosol, may be the main reasons for the heavy haze episode. Light scattering apportionment showed that organic, sulfate containing components, ammonium nitrate and ammonium chloride contributed to light scattering fractions of 54%, 24%, 12% and 10%, respectively. Considering their dominant fractional contribution to light scattering and light extinction, our study indicated that organic components also played an important role in visibility degradation during the winter haze episode in Beijing.

Acknowledgment

We acknowledge Professor Zhang Wu of Lanzhou University for help in nephelometer maintenance. We also acknowledge NOAA and University of Wyoming for backward trajectory calculations and meteorological upper air data analysis, respectively. This work was supported by National Natural Science Foundation of China (41230642), the CAS Strategic Priority Research Program grant XDA05100100 and XDB05020402.

Reference

Anderson, T.L. et al., 2003. Atmospheric science. Climate forcing by aerosol--a hazy picture. Science, 300(5622): 1103-4.

Anderson, T. L., and Ogren, J. A.: Determining Aerosol Radiative Properties Using the Tsi 3563 Integrating Nephelometer, Aerosol Science and Technology, 29, 57-69, 10.1080/02786829808965551, 1998

Andrews, E. et al., 2006. Comparison of methods for deriving aerosol asymmetry parameter. Journal of Geophysical Research, 111(D5).

Beddows, D.C.S., Dall'osto, M. and Harrison, R.M., 2010. An Enhanced Procedure for the Merging of Atmospheric Particle Size Distribution Data Measured Using Electrical Mobility and Time-of-Flight Analysers. Aerosol Science and Technology, 44(11): 930-938.

Chan, Y.C. et al., 1999. Source apportionment of visibility degradation problems in Brisbane (Australia) using the multiple linear regression techniques. Atmospheric Environment, 33(19): 3237-3250.

Chen, J. et al., 2012. A parameterization of low visibilities for hazy days in the North China Plain. Atmospheric Chemistry and Physics, 12(11): 4935-4950.

Chen, J., Zhao, C.S., Ma, N. and Yan, P., 2014. Aerosol hygroscopicity parameter derived from the light scattering enhancement factor measurements in the North China Plain. Atmos. Chem. Phys., 14(15): 8105-8118.

Cheng, Y.F. et al., 2012. Size-resolved measurement of the mixing state of soot in the megacity Beijing, China: diurnal cycle, aging and parameterization. Atmospheric Chemistry and Physics, 12(10): 4477-4491.

Dall'Osto, M., Harrison, R.M., Coe, H. and Williams, P., 2009. Real-time secondary aerosol formation during a fog event in London. Atmos. Chem. Phys., 9(7): 2459-2469.

Deng, Z.Z. et al., 2013. Examination of parameterizations for CCN number concentrations based on in-situ aerosol activation property measurements in the North China Plain. Atmospheric Chemistry and Physics Discussions, 13(1): 145-176.

Garland, R.M. et al., 2008. Aerosol optical properties in a rural environment near the mega-city Guangzhou, China: implications for regional air pollution, radiative forcing and remote sensing. Atmos. Chem. Phys., 8(17): 5161-5186.

Ge, X., Zhang, Q., Sun, Y., Ruehl, C.R. and Setyan, A., 2012. Effect of aqueous-phase processing on aerosol chemistry and size distributions in Fresno, California, during wintertime. Environmental Chemistry, 9(3): 221.

Gysel, M. et al., 2007. Closure study between chemical composition and hygroscopic growth of aerosol particles during TORCH2. Atmos. Chem. Phys., 7(24): 6131-6144.

He, X. et al., 2009. An intensive study of aerosol optical properties in Beijing urban area. Atmos. Chem. Phys., 9: 8903–8915

Hu, M., He, L., Huang, X. and Wu, Z,: Chmeical and physical properties, source and formation of fine and ultrafine particle in Beijing, Science Press, 2009.

Huang, K. et al., 2010a. Relation between optical and chemical properties of dust aerosol over Beijing, China. Journal of Geophysical Research, 115.

Huang, X.F. et al., 2010b. Highly time-resolved chemical characterization of atmospheric submicron particles during 2008 Beijing Olympic Games using an Aerodyne High-Resolution Aerosol Mass Spectrometer. Atmospheric Chemistry and Physics, 10(18): 8933-8945.

Kaufman, Y.J., Koren, I., Remer, L.A., Rosenfeld, D. and Rudich, Y., 2005. The effect of smoke, dust, and pollution aerosol on shallow cloud development over the Atlantic Ocean. Proc Natl Acad Sci U S A, 102(32): 11207-12.

Kim, Y. J., Spak, S. N., Carmichael, G. R., Riemer, N. and Stanier, C. O., 2014. Modeled aerosol

nitrate formation pathways during wintertime in the Great Lakes region of North America. Journal of Geophysical Research:Atmospheres, **DOI:** 10.1002/2014JD022320

Koren, I., Kaufman, Y.J., Rosenfeld, D., Remer, L.A. and Rudich, Y., 2005. Aerosol invigoration and restructuring of Atlantic convective clouds. Geophysical Research Letters, 32(14): n/a-n/a.

Li, W.J., Shao, L.Y. and Buseck, P.R., 2010. Haze types in Beijing and the influence of agricultural biomass burning. Atmospheric Chemistry and Physics, 10(17): 8119-8130.

Liu, X.G. et al., 2013. Formation and evolution mechanism of regional haze: a case study in the megacity Beijing, China. Atmospheric Chemistry and Physics, 13(9): 4501-4514.

Liu, Z. et al., 2015. Seasonal and diurnal variation in particulate matter (PM10 and PM2.5) at an urban site of Beijing: analyses from a 9-year study. Environmental Science and Pollution Research, 22(1): 627-642.

Liu, Z.R., Hu, B., Liu, Q., Sun, Y. and Wang, Y.S., 2014. Source apportionment of urban fine particle number concentration during summertime in Beijing. Atmospheric Environment(0).

Lohmann, U. and Feichter, a.J., 2005. Global indirect aerosol effects: a review. Atmos. Chem. Phy. , 5: 715-737.

Liou, K.N.: An introduction to atmospheric radiation (second edition), Elsevier Science, 2002.

Lowenthal, D.H., Rogers, C.F., Saxena, P., Watson, J.G. and Chow, J.C., 1995. Sensitivity of estimated light extinction coefficients to model assumptions and measurement errors. Atmospheric Environment, 29(7): 751-766.

Ma, N. et al., 2012. A new method to determine the mixing state of light absorbing carbonaceous using the measured aerosol optical properties and number size distributions. Atmospheric Chemistry and Physics, 12(5): 2381-2397.

Meier, J. et al., 2009. Hygroscopic growth of urban aerosol particles in Beijing (China) during wintertime: a comparison of three experimental methods. Atmos. Chem. Phys., , 9: 6865–6880

Nel, A., 2005. Atmosphere. Air pollution-related illness: effects of particles. Science, 308(5723): 804-6.

Pan, X.L. et al., 2009. Observational study of influence of aerosol hygroscopic growth on scattering coefficient over rural area near Beijing mega-city. Atmos. Chem. Phys. , 9: 7519–7530.

Pitchford, M. et al., 2007. Revised Algorithm for Estimating Light Extinction from IMPROVE Particle Speciation Data. Journal of the Air & Waste Management Association, 57(11): 1326-1336.

Poschl, U., 2005. Atmospheric aerosols: composition, transformation, climate and health effects. Angew Chem Int Ed Engl, 44(46): 7520-40.

Qu, W.J. et al., 2010. Spatial distribution and interannual variation of surface PM₁₀ concentrations over eighty-six Chinese cities. Atmospheric Chemistry and Physics, 10(12): 5641-5662.

Quan, J. et al., 2011. Analysis of the formation of fog and haze in North China Plain (NCP). Atmospheric Chemistry and Physics, 11(15): 8205-8214.

Ramanathan, V., Crutzen, P.J., Kiehl, J.T. and Rosenfeld, D., 2001. Aerosols, climate, and the hydrological cycle. Science, 294(5549): 2119-24.

Sakurai, H. et al., 2005. Hygroscopicity and volatility of 4–10 nm particles during summertime atmospheric nucleation events in urban Atlanta. Journal of Geophysical Research: Atmospheres, 110(D22): D22S04.

Seinfeld, J. H., and Pandis, S. N.: Atmospheric Chemistry and physics, From Air Pollution to Climate Changes, Wiley, New York, USA, 1998.

Shi, J.P., Evans, D.E., Khan, A.A. and Harrison, R.M., 2001. Sources and concentration of nanoparticles (<10 nm diameter) in the urban atmosphere. Atmospheric Environment, 35(7): 1193-1202.

Sun, Y.L., Zhuang, G.S., T ang , A., Wang, Y. and And An, Z., 2006. Chemical Characteristics of PM2.5 and PM10 in Haze-fog Episodes in Beijing. Environ. Sci. Technol., 40: 3148-3155.

Tang, G. et al., 2012. Spatial-temporal variations in surface ozone in Northern China as observed during 2009–2010 and possible implications for future air quality control strategies. Atmos. Chem. Phys., 12(5): 2757-2776.

Titos, G. et al., 2012. Optical properties and chemical composition of aerosol particles at an urban location: An estimation of the aerosol mass scattering and absorption efficiencies. Journal of Geophysical Research: Atmospheres, 117(D4): D04206.

Twomey, S., 1977. The Influence of Pollution on the Shortwave Albedo of Clouds. Journal of the Atmospheric Sciences, 34: 1149-1152.

Wang, K.C., Dickinson, R.E., Su, L. and Trenberth, K.E., 2012a. Contrasting trends of mass and optical properties of aerosols over the Northern Hemisphere from 1992 to 2011. Atmospheric Chemistry and Physics, 12(19): 9387-9398.

Wang, L. et al., 2012b. Understanding haze pollution over the southern Hebei area of China using the CMAQ model. Atmospheric Environment, 56: 69-79.

Wang, Y. et al., 2013. Mechanism for the formation of the January 2013 heavy haze pollution episode over central and eastern China. Science China Earth Sciences.

Wang, Y.H. et al., 2014. Ozone weekend effects in the Beijing–Tianjin–Hebei metropolitan area, China. Atmos. Chem. Phys., 14(5): 2419-2429.

Watson, J.G., 2002. Visibility: Science and Regulation. Journal of the Air & Waste Management Association, 52(6): 628-713.

Wehner, B. et al., 2008. Relationships between submicrometer particulate air pollution and air mass history in Beijing, China, 2004–2006. Atmos. Chem. Phys., 8: 6155–6168.

Wu, Z. et al., 2007. New particle formation in Beijing, China: Statistical analysis of a 1-year data set. Journal of Geophysical Research, 112(D9).

Yang, M., Howell, S.G., Zhuang, J. and Huebert, a.B.J., 2009. Attribution of aerosol light absorption to black carbon, brown carbon, and dust in China – interpretations of atmospheric measurements during EAST-AIRE. Atmos. Chem. Phys.,, 9: 2035–2050.

Yao, T. et al., 2010. High time resolution observation and statistical analysis of atmospheric light extinction properties and the chemical speciation of fine particulates. SCIENCE CHINA Chemistry, 53(8): 1801-1808.

Zhang, J.K. et al., 2014. Characterization of submicron aerosols during a month of serious pollution in Beijing, 2013. Atmos. Chem. Phys., 14(6): 2887-2903.

Zhang, Q., Quan, J., Tie, X., Huang, M. and Ma, X., 2011. Impact of aerosol particles on cloud formation: Aircraft measurements in China. Atmospheric Environment, 45(3): 665-672.

Zhang, Q. et al., 2004. Insights into the Chemistry of New Particle Formation and Growth Events in Pittsburgh Based on Aerosol Mass Spectrometry. Environmental Science & Technology, 38(18): 4797-4809.

Zhang, Q.H., Zhang, J.P. and Xue, H.W., 2010. The challenge of improving visibility in Beijing. Atmospheric Chemistry and Physics, 10(16): 7821-7827.

Zhang, X. et al., 2013. Factors contributing to haze and fog in China. Chinese Science Bulletin (Chinese Version), 58(13): 1178.

Zhang, X.Y. et al., 2012. Atmospheric aerosol compositions in China: spatial/temporal variability, chemical signature, regional haze distribution and comparisons with global aerosols. Atmospheric Chemistry and Physics, 12(2): 779-799.

Zhao, X.J. et al., 2013. Analysis of a winter regional haze event and its formation mechanism in the North China Plain. Atmospheric Chemistry and Physics, 13(11): 5685-5696.

550

551

552

553 Table 1 The statistic of aerosol optical properties during observation period.

Parameter	mean	median	Standard derivation	5% quantile	95% quantile
σ_{sp}^{450} (Mm^{-1})	1088.5	924.4	748.1	48.1	2386.3
σ_{sp}^{550} (Mm^{-1})	877.2	748.4	624.2	36.6	1993.4
σ_{sp}^{700} (Mm^{-1})	718.4	628.2	530.9	28.7	1703.3
σ_{bsp}^{450} (Mm^{-1})	134.4	122.8	87.1	7.6	281.4
σ_{bsp}^{550} (Mm^{-1})	108.1	96.4	71	6.1	228.5
σ_{bsp}^{700} (Mm^{-1})	98.7	89.3	66.5	7.3	214.4
b_{450}	0.13	0.13	0.02	0.11	0.16
b_{550}	0.14	0.12	0.02	0.11	0.17
b_{700}	0.15	0.14	0.02	0.13	0.19
$\overset{0}{A}_{450/550}$	1.2	1.3	0.3	0.74	1.7
$\overset{0}{A}_{550/700}$	0.94	1.0	0.3	0.41	1.4
g_{450}	0.58	0.6	0.04	0.52	0.62
g_{550}	0.57	0.6	0.05	0.50	0.63
g_{700}	0.54	0.56	0.05	0.46	0.60

554

555

556 Table 2 The statistic of particle number concentration during observation period.

Parameter	Mean	median	Standard derivation	5% quantile	95% quantile
Nucleation(cm^{-3})	1.90×10^{5}	1.8×10^{5}	8.3×10^{4}	6.3×10^{4}	3.4×10^{5}
Aitken(cm^{-3})	1.5×10^{6}	1.4×10^{6}	6.4×10^{5}	5.7×10^{5}	2.7×10^{6}
Accumulation(cm^{-3})	1×10^{6}	9.9×10^{6}	3.9×10^{5}	4.7×10^{5}	1.6×10^{6}
Coarse (cm^{-3})	3.1×10^{3}	2.9×10^{3}	2.3×10^{3}	2.5×10^{2}	7.0×10^{3}

557

558

559

560

561

562

563

564

565

566

567

568

569

570

571

572

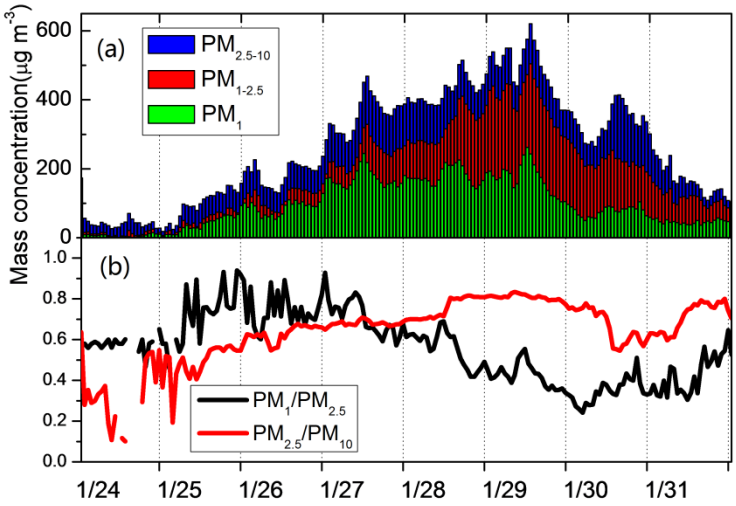

Figure 1 Time series of (a) mass concentrations of PM_1, $PM_{1\text{-}2.5}$ and $PM_{2.5\text{-}10}$, (b) mass ratios of $PM_1/PM_{2.5}$ and $PM_{2.5}/PM_{10}$

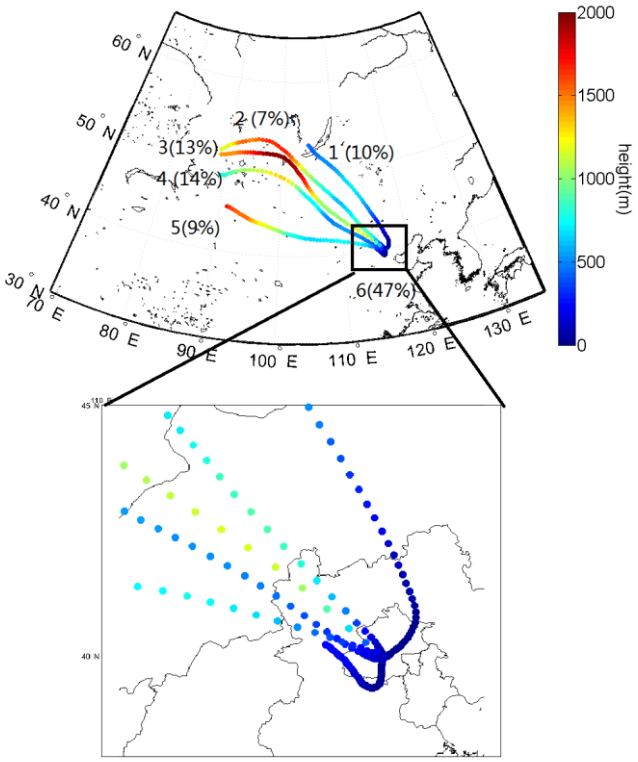

Figure 2 The three days backward trajectory of air parcels during the observation period; the colors of air trajectories represent height during transport.

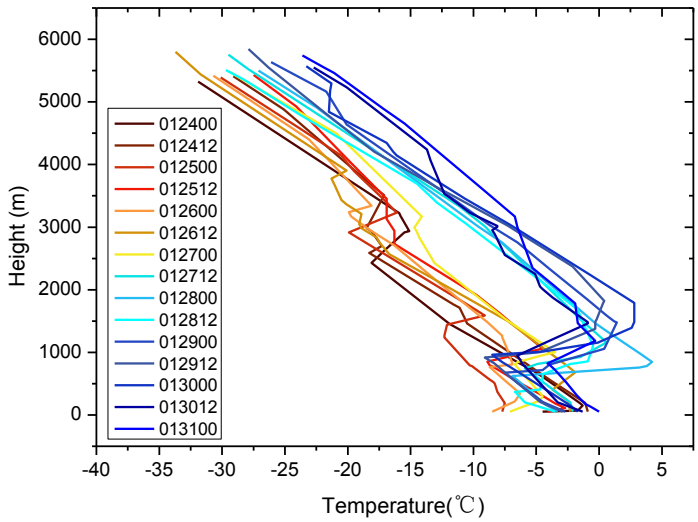

Figure 3 The temperature profiles during observation period. The legend stands for UTC time. For example, 012400 means 0:00 on January 24th.

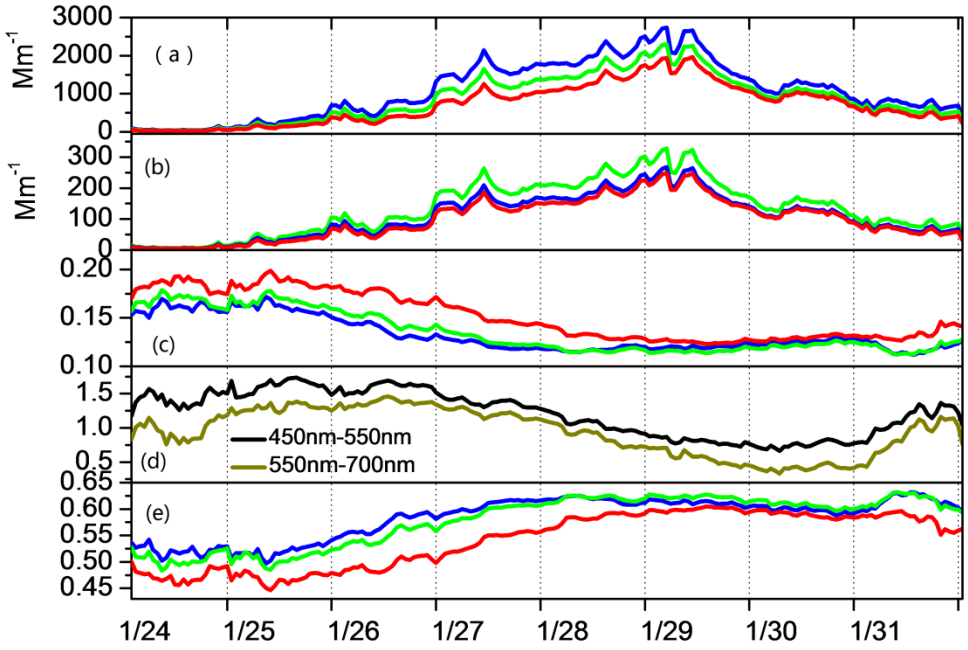

Figure 4 Time series of (a) scattering coefficients σ_{sp}, (b) backscattering coefficients σ_{bsp}, (c) backscattering ratios b_{λ}, (e) asymmetry parameter g_{λ} at wavelengths of 450nm (blue), 550nm (green) and 700nm (red) (d) scattering Ångström exponent ($Å_{sp}$) from 450nm-550nm (black) and 550nm-700nm(brown).

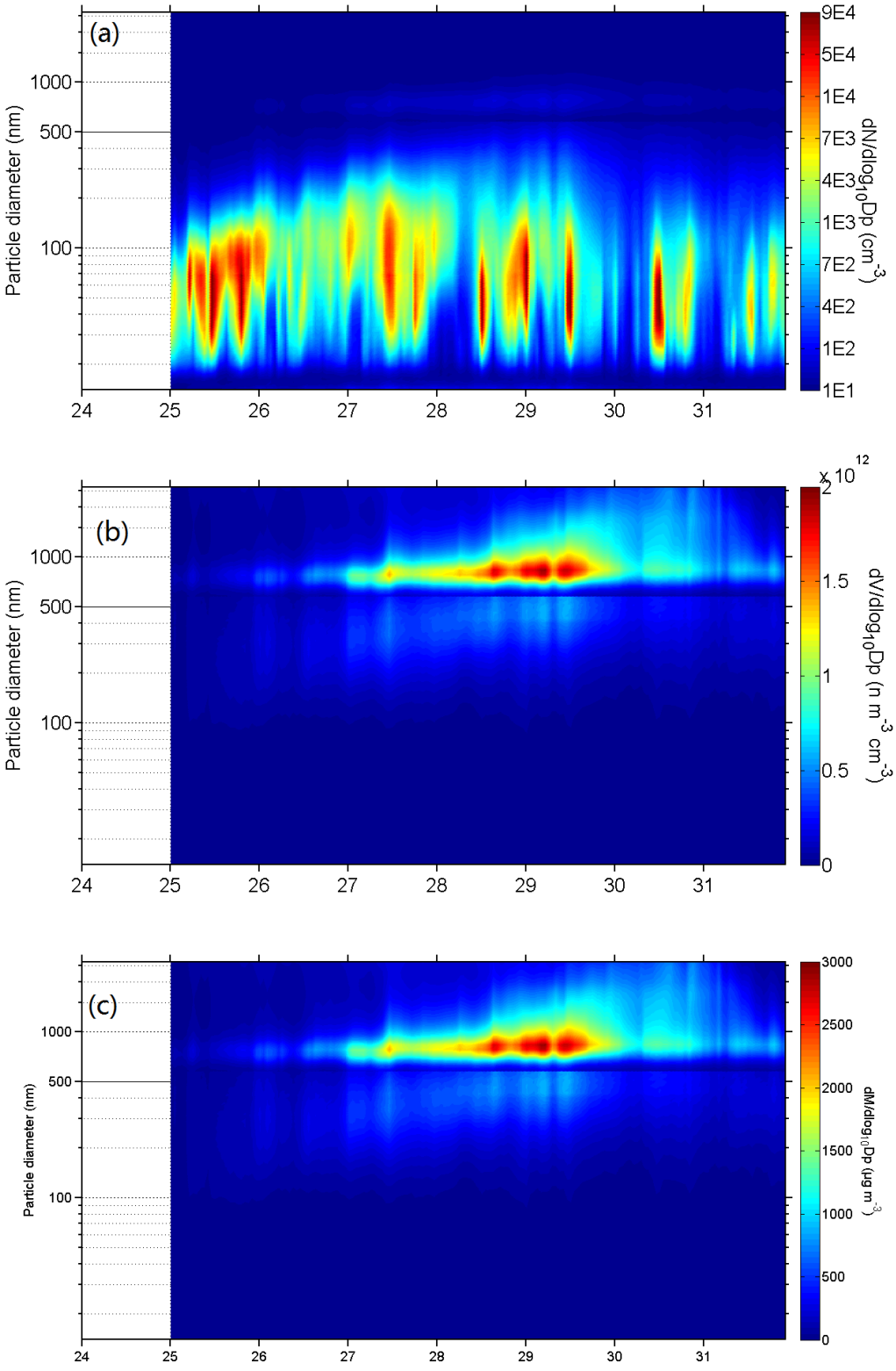

Figure 5Time series of (a) particle number size distribution (b) particle volume size distribution (c) particle mass size distribution between 14.1nm-2458nm using SMPS combined with APS from January 25 to 31.The x-axis represents the data of January

and y-axis represents particle diameter (nm). The color in the figure 3 represents particle concentration (dN/dlog D_p).

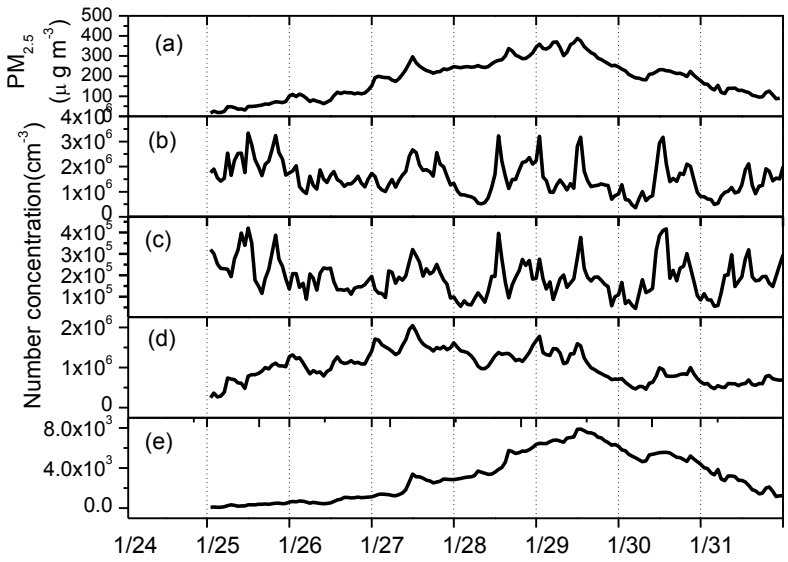

Figure 6 Time series of (a) particle mass concentration calculated from number size distribution and number concentrations of (b) nucleation mode (14.1nm-25nm), (c) Aitken mode (25nm-100nm), (d) accumulation mode (100nm-1000nm) and (e) coarse mode (1000nm-2458nm) from January 25 to January 31.

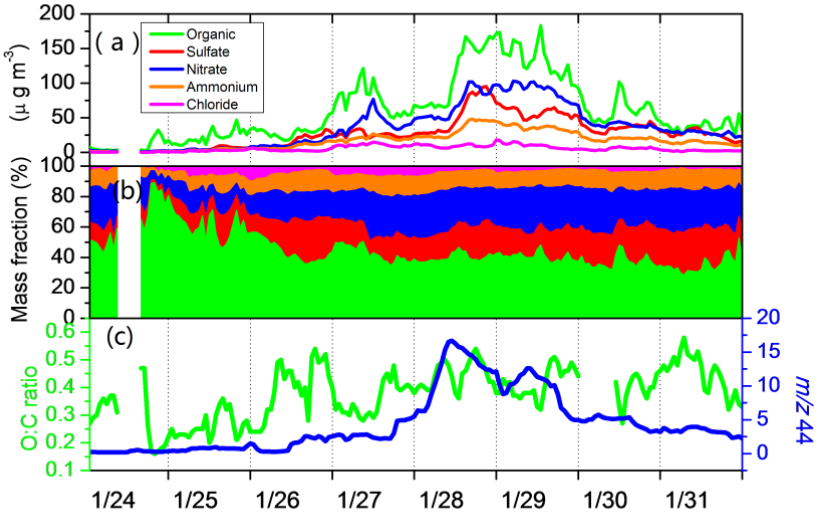

Figure 7 Time series of (a) mass concentrations of organic, sulfate, nitrate, ammonium and chloride in submicron aerosol (b) mass fractions of organic, sulfate, nitrate, and ammonium and chloride (c) O: C ratio and m/z 44 during the haze episode.

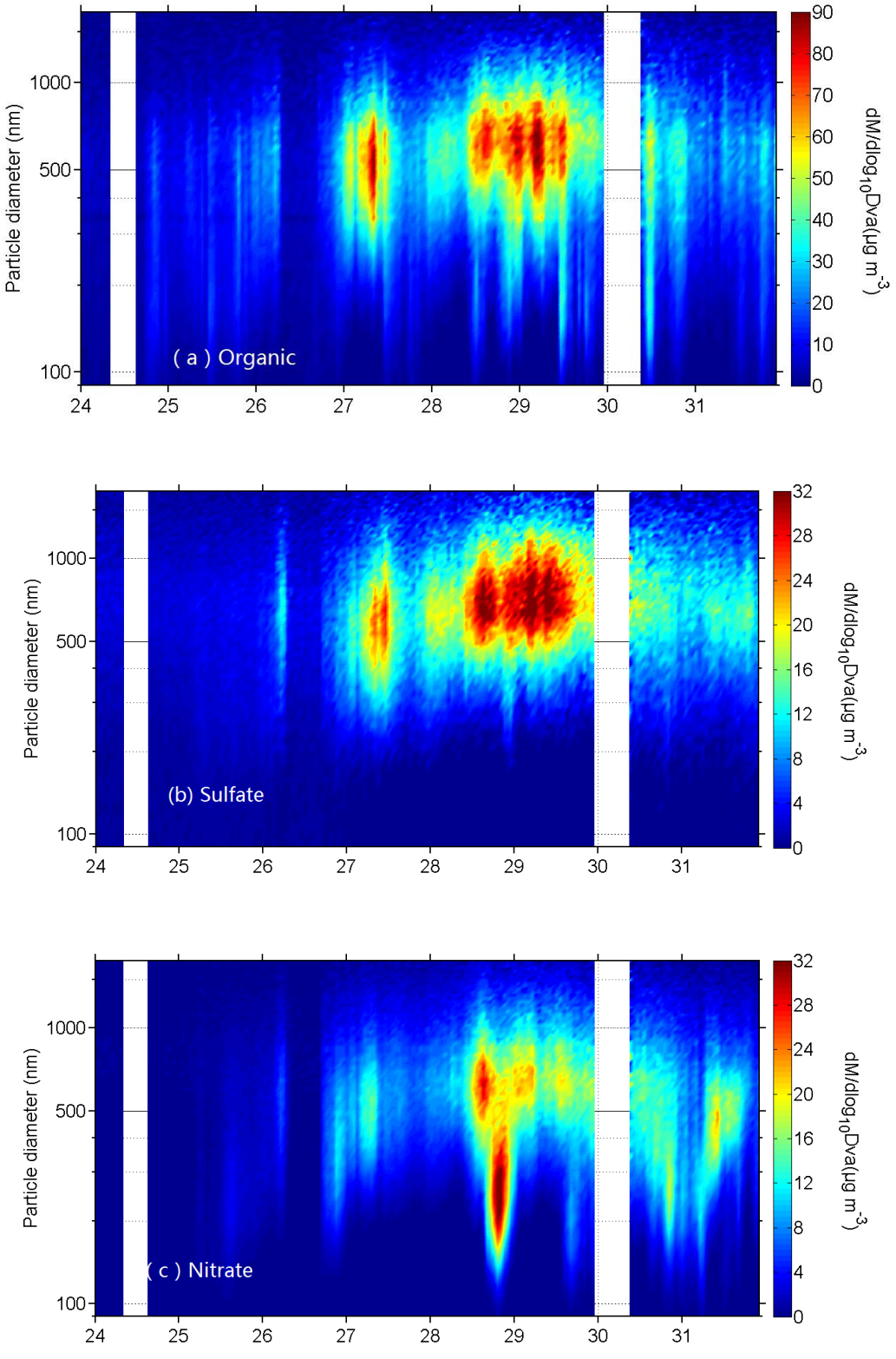
Particle diameter (nm)
1000
500
100
24
25
26
27
28
29
30
31
(a) Organic
(b) Sulfate
(c) Nitrate
dM/dlog10Dva(μg m-3)
90
80
70
60
50
40
30
20
10
0
32
28
24
20
16
12
8
4
0

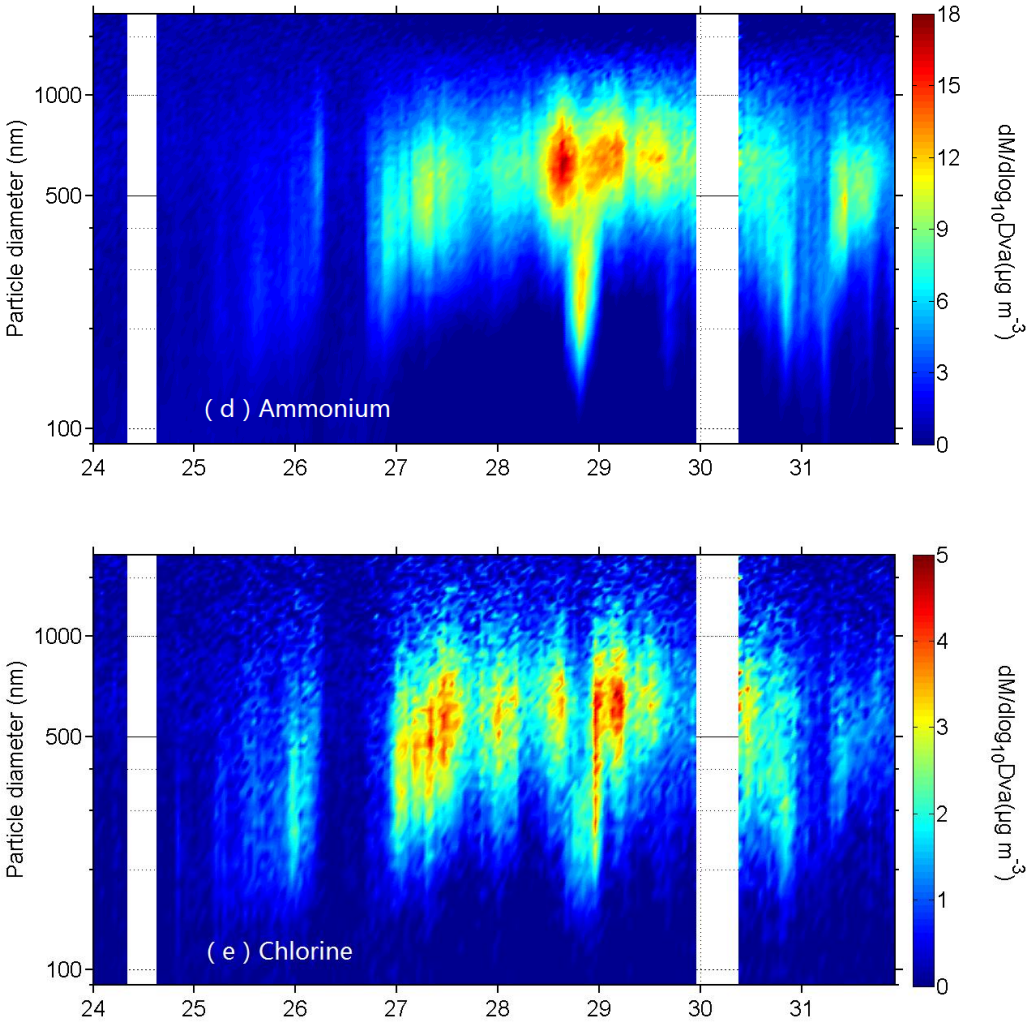

Figure 8 Size-resolved chemical compositions of (a) organic (b) sulfate (c) nitrate (d) ammonium and (e) chlorine

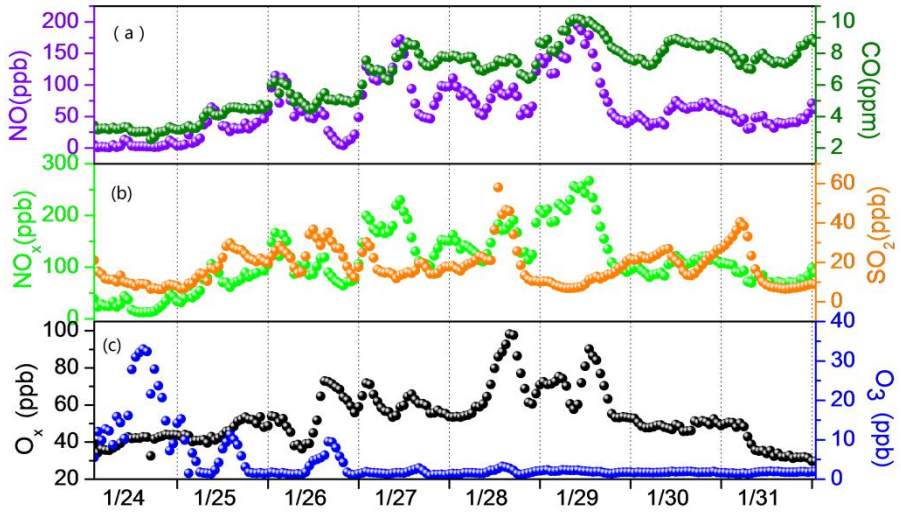

Figure 9 Mixing ratios of (a) NO and CO (b) NO_x and SO_2 (c) O_x and O_3

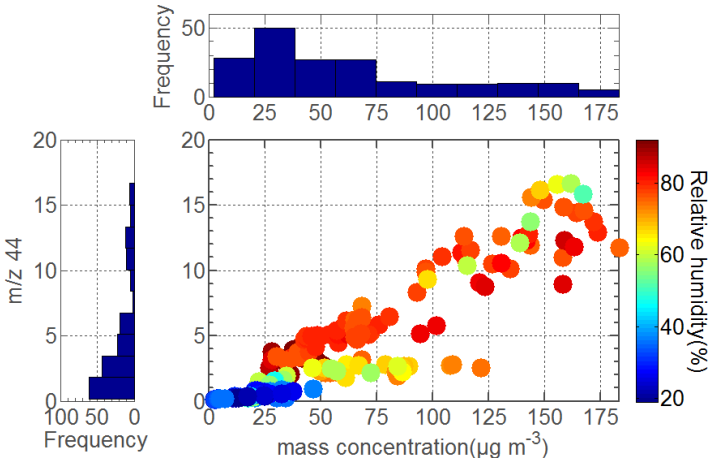

Figure 10 (left panel) the frequency distribution of m/z 44, (top panel) the frequency distribution of organic mass, (center panel) abundance of m/z 44 as a function of organic aerosol mass concentration and the influence of RH (left, color scale).

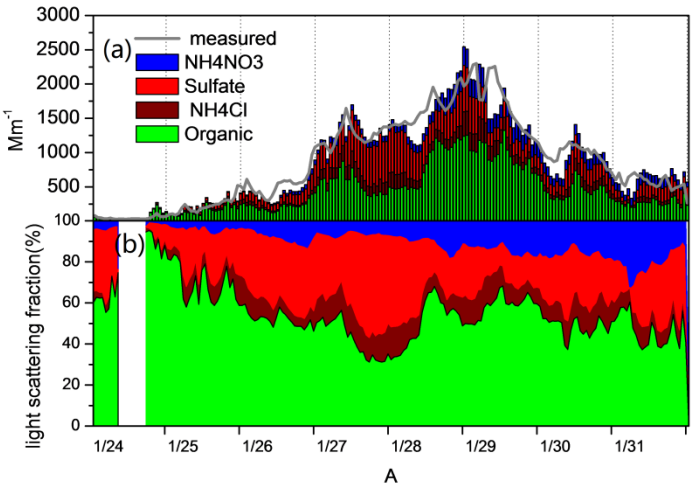

Figure 11 Time series of (a) apportioned light scattering coefficients of each aerosol components compared with measured (b) light scattering fractions of each aerosol components.

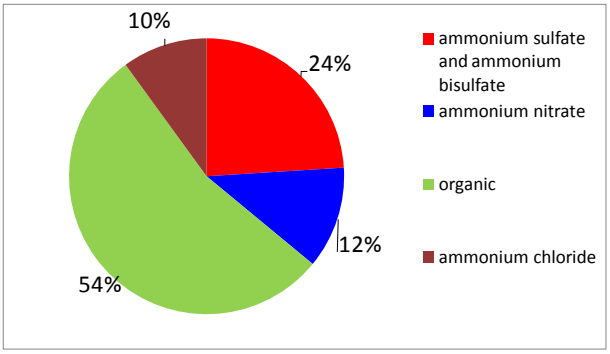

Figure 12 Averaged light scattering contribution of each aerosol components during the haze episode